

## Near-Field Thermophotovoltaic System Design and Calculation based on Coupled-Mode Analysis

Wang, B.; Lin, C.; Teo, K.H.

TR2017-227 October 2017

### Abstract

The coupling of resonant modes between two surfaces is important in near-field heat transfer and near-field thermophotovoltaic (TPV) systems. Recently, coupled-mode theory (CMT) has been developed for the analysis and optimal design of TPV systems. In this paper, we use CMT to analyze the "emitter-vacuum-PV cell" configuration, and quantitatively show that how the emitter of a nanostructure can drastically improve the near-field TPV device performance. The key feature of the nanostructure is the additional geometry-induced resonant mode, whose energy is lower than the original surface plasmon polariton (SPP) resonant frequency and much closer to the bandgap of the PV cell. Specifically, we show that with a simple grating structure, the generated power density of a TPV cell is increased from 13 W/cm<sup>2</sup> to 34 W/cm<sup>2</sup> when the PV cell is fixed at 300 K and the emitter 1000 K. The increase is over 20 times higher when both planar and grating emitters are at a lower temperature of 500 K.

*Journal of Photonics for Energy*

This work may not be copied or reproduced in whole or in part for any commercial purpose. Permission to copy in whole or in part without payment of fee is granted for nonprofit educational and research purposes provided that all such whole or partial copies include the following: a notice that such copying is by permission of Mitsubishi Electric Research Laboratories, Inc.; an acknowledgment of the authors and individual contributions to the work; and all applicable portions of the copyright notice. Copying, reproduction, or republishing for any other purpose shall require a license with payment of fee to Mitsubishi Electric Research Laboratories, Inc. All rights reserved.



# Near-Field Thermophotovoltaic System Design and Calculation based on Coupled-Mode Analysis

Bingnan Wang<sup>a,\*</sup>, Chungwei Lin<sup>a</sup>, Koon Hoo Teo<sup>a</sup>

<sup>a</sup>Mitsubishi Electric Research Laboratories, 201 Broadway Ste 8, Cambridge, MA 02139 USA

## Abstract.

The coupling of resonant modes between two surfaces is important in near-field heat transfer and near-field thermophotovoltaic (TPV) systems. Recently, coupled-mode theory (CMT) has been developed for the analysis and optimal design of TPV systems. In this paper, we use CMT to analyze the “emitter-vacuum-PV cell” configuration, and quantitatively show that how the emitter of a nanostructure can drastically improve the near-field TPV device performance. The key feature of the nanostructure is the additional geometry-induced resonant mode, whose energy is lower than the original surface plasmon polariton (SPP) resonant frequency and much closer to the bandgap of the PV cell. Specifically, we show that with a simple grating structure, the generated power density of a TPV cell is increased from 13 W/cm<sup>2</sup> to 34 W/cm<sup>2</sup> when the PV cell is fixed at 300 K and the emitter 1000 K. The increase is over 20 times higher when both planar and grating emitters are at a lower temperature of 500 K.

**Keywords:** radiative transfer, near-field, thermophotovoltaic.

\*Bingnan Wang, [bwang@merl.com](mailto:bwang@merl.com)

## 1 Introduction

Near-field radiation is an important heat transfer mechanism that has great potential in many applications, including thermal imaging, sensing, radiative cooling, and energy conversion in thermophotovoltaic (TPV) systems.<sup>1-3</sup> A TPV system converts heat into electricity through thermal radiation,<sup>4-11</sup> and consists of a thermal emitter and a semiconductor photovoltaic (PV) cell. A heat source keeps the thermal emitter at a high temperature, and generates thermal radiation, which is then absorbed by the PV cell with bandgap energy  $E_g = \hbar\omega_g$ .<sup>6-8</sup> Photons with energy lower than  $E_g$  cannot generate conducting electrons and are unusable; photons with energy much higher than  $E_g$  can generate electron-hole pairs, but the additional energy higher than  $E_g$  contributes to thermal loss and is wasted. Therefore, assuming all photons with energy larger than  $E_g$  absorbed by the PV cell generates an electron-hole pair, Carnot efficiency limit can only be reached with monochromatic radiation from the emitter that is matched to  $E_g$ .<sup>4,5</sup>

However, for a far-field based TPV system, where the distance between the emitter and the PV cell is much larger than the characteristic wavelength of photons, the emission power is limited by the blackbody radiation, and the emissivity cannot exceed unity at any given frequency. Therefore, the emission power from the emitter would be infinitesimally small assuming a monochromatic radiation spectrum. Instead, the design target for an ideal thermal emitter for far-field TPV is to have emissivity to be unity above bandgap, and zero below bandgap. Various approaches have been proposed to engineer the emission spectrum toward this target, with nanostructured photonic designs including microcavities, photonic crystals, and gratings.<sup>12-16</sup> On the other hand, the near-field based radiative heat transfer can exceed the blackbody limit due to the contributions from evanescent modes.<sup>17-20</sup> In particular, when resonant modes are supported by the emitter and/or absorber, and the separation between the emitter and absorber is a fraction of the wavelength determined by the resonant modes, the absorption spectrum has strong peaks at resonant energies with intensity a few orders exceeding the blackbody limit.<sup>18,21</sup> Various materials and nanostructures have

been investigated for enhancing the near-field radiative transfer with resonant coupling.<sup>22–24</sup> Near-field based TPV systems have also been proposed for improving the power density and efficiency by utilizing resonant modes such as surface phonon polaritons and surface plasmon polaritons (SPPs).<sup>22,25–30</sup> The analysis of resonant modes is therefore critical for near-field radiation based system.

Conventionally, radiative heat transfer between an emitter and an absorber is quantified using dyadic Green function and the fluctuation-dissipation theorem.<sup>17–19</sup> The approach is rigorous, but the resulting expressions are complicated and not straightforward to analyze. Recently, coupled-mode theory (CMT) has been developed for emitters supporting resonant modes,<sup>31</sup> and radiative heat transfer in a near-field TPV system.<sup>32</sup> The CMT facilitates the design of near-field TPV system configurations toward higher power density and efficiency.<sup>33</sup> Optimal designs with impedance matching principal for different material systems have also been investigated.<sup>34</sup> So far the CMT is limited to the mode analysis of the TPV system. The important performance parameters of the system, including emissivity, radiation power and output electric power are still calculated with dyadic Green function and the fluctuation-dissipation theorem. And the proposed systems are limited to planar layered configurations. For periodically structured surfaces, effective medium approach is typically used to approximate the structures as a medium with flat surface with effective material properties.<sup>35,36</sup> It was shown recently that this method fails to predict the near-field radiative transfer behavior due to certain geometry-induced resonant modes.<sup>24</sup>

In this paper, we calculate all performance parameters of a near-field TPV system including transmissivity, radiation power, electric power, and efficiency based on resonant modes supported by the system. Furthermore, we expand the calculation to systems with periodic nanostructures supporting additional resonant modes. We show that these modes are captured using CMT method, and can bring the resonant peak closer to the bandgap energy  $E_g$  of a typical TPV cell, therefore increasing the radiative heat transfer rate, and the output electric power.

## 2 Coupled-Mode Analysis

Consider a TPV system with an emitter and a TPV cell, for each resonant mode it supports, according to CMT,<sup>32</sup> the thermal transmissivity between loss mechanism  $i$  and  $j$  can be calculated from the resonant frequency  $\omega_0$  and the loss rates (the  $\Gamma$  terms) associated with each loss mechanism.

$$\epsilon_{ij}(\omega) = \epsilon_{ji}(\omega) = \frac{4\Gamma_i\Gamma_j}{(\omega - \omega_0)^2 + (\sum_n \Gamma_n)^2} \quad (1)$$

For a system supporting multiple resonant modes that are orthogonal, the transmissivity is simply the summation of the transmissivity for each mode. For a planar system, different resonant modes are supported for each in-plane (xy plane) wavevector  $k$ , and the overall transmissivity per unit area is calculated by summing up all  $k$  contributions  $\epsilon_{ij}(\omega) = \int_0^\infty \frac{kdk}{2\pi} \epsilon_{ij}(\omega, k)$  for continuous  $k$ , and can be evaluated using  $\epsilon_{ij}(\omega) = \sum_0^\infty \frac{k\delta k}{2\pi} \epsilon_{ij}(\omega, k)$  on the discretized  $k$ -points. Here the in-plane rotational symmetry is used. For system with periodic structures of pitch  $p$  in x-direction, while continuous in y-direction, the  $k_x$  integral is modified to  $\int_{-\infty}^\infty dk_x \rightarrow \sum_{n_x} \int_{-\pi/p}^{\pi/p} dk_x$ , with  $n_x$  being the band index. The summation for the transmissivity is thus changed to  $\epsilon_{ij}(\omega) = \frac{4}{(2\pi)^2} \sum_{n_x} \int_0^\infty \int_0^{\pi/p} dk_x dk_y \epsilon_{ij,n_x}(\omega, k_x, k_y)$ , or  $\epsilon_{ij}(\omega) = \sum_{n_x} \frac{4}{(2\pi)^2} \sum_0^\infty \sum_0^{\pi/p} \delta k_x \delta k_y \epsilon_{ij,n_x}(\omega, k_x, k_y)$ . The thermal emissivity from an object is the summation of transmissivity to all other loss mechanisms:  $\epsilon_i(\omega) = \sum_{j \neq i} \epsilon_{ij}(\omega)$ .

We consider a general case where the thermal emitter  $e$  is at a higher temperature of  $T_1$ , and the PV absorber is at a lower temperature  $T_2$ , surrounded by the background  $b$  at the same temperature  $T_2$ . The thermal sources in a lossy object at temperature  $T$  and chemical potential  $qV$  is described by the generalized Planck distribution:  $\Theta_{VT}(\omega) = \frac{1}{\exp[(\hbar\omega - qV)/k_B T] - 1}$ , and the PV cell absorbs photons via several loss mechanisms.<sup>4,32</sup> Following Ref.<sup>32</sup> we distinguish two types of loss mechanisms. The desired interband absorption  $g$ , associated with the bandgap, leads to a voltage  $V$  across the TPV cell and a photogenerated current  $I$  into external load  $l$ . The thermal radiation associated with  $g$  is described by  $\Theta_{VT_2}(\omega)$ . All other loss mechanisms do not generate  $V$  and  $I$ , with generated photons described by  $\Theta_{0T_2}(\omega)$ , and are incorporated in the background loss  $b$ .

Subsequently, the radiative transfer power density between two planar surfaces due to loss mechanism  $i$  and  $j$  is quantified as

$$q'' = \int_0^\infty \frac{d\omega}{2\pi} \hbar\omega [\Theta_{V_i T_i}(\omega) - \Theta_{V_j T_j}(\omega)] \epsilon_{ij}(\omega) \quad (2)$$

The power outflow from the emitter  $P_e(V)$ , and the power generated onto the load  $P_l$  are both functions of the voltage  $V$  of the cell, and can be calculated by considering the loss mechanisms terms separately.

$$P_e(V) = \int_0^\infty \frac{d\omega}{2\pi} \hbar\omega \left\{ [\Theta_{0T_1}(\omega) - \Theta_{VT_2}(\omega)] \epsilon_{eg}(\omega) + [\Theta_{0T_1}(\omega) - \Theta_{0T_2}(\omega)] \epsilon_{eb}(\omega) \right\} \quad (3)$$

$$P_l(V) = qV \int_0^\infty \frac{d\omega}{2\pi} \left\{ [\Theta_{0T_1}(\omega) - \Theta_{VT_2}(\omega)] \epsilon_{eg}(\omega) + [\Theta_{0T_2}(\omega) - \Theta_{VT_2}(\omega)] \epsilon_{gb}(\omega) \right\} \quad (4)$$

And the power conversion efficiency is simply the ratio of the two:  $\eta = P_l/P_e$ .<sup>32</sup>

Mathematically the lossy terms are reflected in the imaginary part of the permittivity of the TPV cell material:  $\epsilon_a = \epsilon'_a + \epsilon''_a = \epsilon'_a + i(\epsilon''_b + \epsilon''_g)$ . We apply the model in Ref.<sup>32</sup> for the PV cell:  $\epsilon' = 14$  for real part of permittivity,  $\epsilon''_g = 0.7 \sqrt{14\omega_g(\omega - \omega_g)}/\omega$  for the interband absorption, and  $\epsilon''_b = 0.1$  to account for the background absorption with no voltage generation. In the following study, we use bandgap energy  $E_g = 0.41\text{eV}$ , which is a typical value for a GaInAsSb based PV cell. The emitter is described by a Drude model as  $\epsilon_e(\omega) = 1 - \omega_p^2/(\omega^2 + i\gamma\omega)$ , where  $\omega_p$  is the plasma frequency, and  $\gamma$  is the damping rate. In our calculations we use  $\omega_p = 1.23\text{eV}$ ,  $\gamma = 0.00246\text{eV}$ , which are associated with refractory metal TiC, which has a high melting temperature of over 3000 K.

We point out in the CMT formalism, only (complex) resonant frequencies are involved, and the spatial distributions of the resonant modes are not required. Therefore, the CMT analysis can give an approximate but quantitative transmissivity, as far as the resonant frequencies are obtained, either from some numerical eigensolver or from experimental measurements.

## 2.1 Calculation Process

To obtain the complex eigenfrequencies, we use the eigenfrequency solver in COMSOL to find the complex-valued eigenmodes for each system. For emitter with periodically arranged nanostructures in the x-direction, one unit cell is modeled in the simulator, with periodic boundary conditions with Floquet periodicity applied to the two ends. A wavevector value  $k_x$  between 0 and  $\pi/p$  is applied to the Floquet periodicity. The structure is infinitely long in the y-direction, and a wavevector

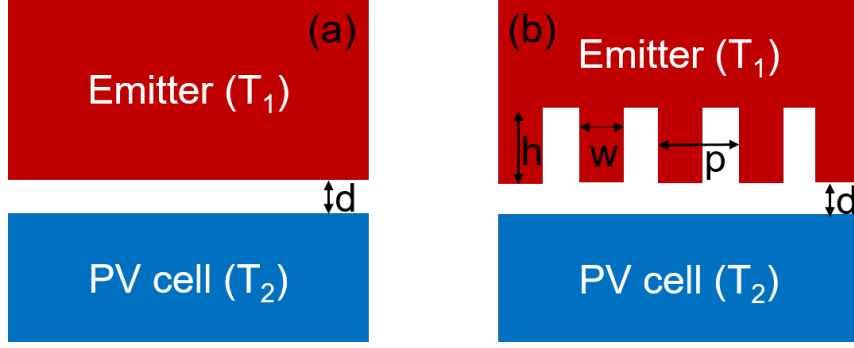


**Fig 1** Structures of near-field TPV system (a) with planar emitter, and (b) with periodically structured emitter:  $h = 60$  nm,  $p = 60$  nm,  $w = 30$  nm.  $d = 10$  nm for both cases.

value  $k_y$  can also be assigned. For each  $k_x$  and  $k_y$  combination, the solver finds the eigenfrequencies and the corresponding damping rates of the supported modes. The damping rate associated with each loss mechanism is obtained by activating the loss in the material properties only, which all other mechanisms are switched off. For example,  $\Gamma_e$  is calculated with the loss terms in the PV material  $\varepsilon_g''$  and  $\varepsilon_b''$  to be zero;  $\Gamma_a$  is calculated by activating the imaginary part of permittivity  $\varepsilon_a''$  while having  $\gamma = 0$  in the Drude model of the emitter. The corresponding transmissivity between two loss mechanisms can then be calculated with Eq. 1. Another simulation is performed with a different set of wavevector values, until all contributions from the  $k$ -space are included. Then the overall transmissivity at each frequency is calculated by integrating over wavevector, and the radiative transfer power density is obtained with another integral over all frequency components, as described in Eq. 2. The power and efficiency can also be calculated similarly.

### 3 Results and Discussions

With this procedure, we have calculated the planar TPV system presented in Ref.,<sup>32</sup> and all major results, including the resonant modes, the transmissivity, the power density, and efficiency, are in good agreement with those obtained rigorously.

We also verified the accuracy of the procedure for 1d grating structures by calculating the near-field radiative heat transfer between two Au gratings, where multiple resonant modes are supported, and comparing the results with those obtained by rigorous coupled-wave analysis (RCWA) as presented in Fig. 2(a) of Ref.<sup>24</sup> The frequency-dependent transmissivity  $\varepsilon(\omega)$  from the grating emitter surface is plotted as a function of the frequency, and the curve obtained from coupled-mode analysis was in good agreement with the exact result in Fig. 2(a) of Ref.<sup>24</sup> Both transmissivity peaks at angular frequencies  $4.5 \times 10^{14}$  rad/s and  $6.5 \times 10^{14}$  rad/s were obtained, with amplitude error within 2% for both peaks.

Next we show that the coupled-mode analysis can be used to calculate the energy conversion in a near-field TPV system with nanostructured patterns. Fig. 1 shows the simulated structures in this study, and the geometrical parameters.

#### 3.1 Planar Emitter

For comparison, the system with planar emitter is calculated first. The surface mode supported by the system is the SPP resonance, which approaches  $\omega_0 = \omega_p/\sqrt{2} = 2.12\omega_g$  at large  $k$ . For

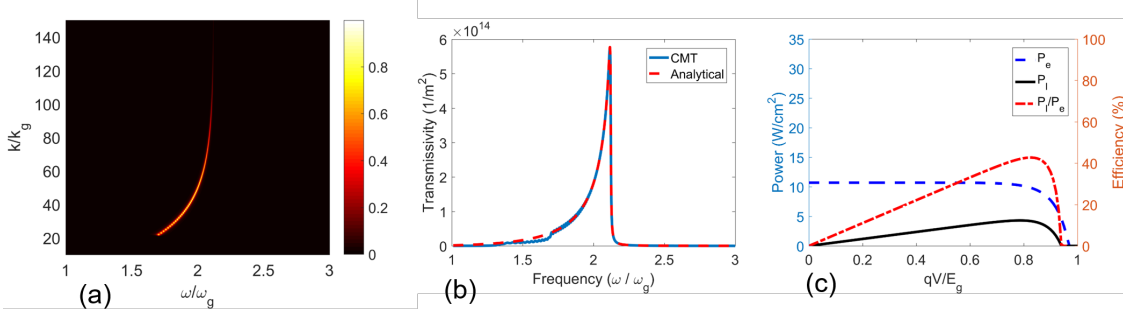


**Fig 2** Coupled-mode calculation results for the planar system: (a) dispersion curve calculated; (b) transmissivity as a function of frequency with both coupled mode theory and analytical method based on Green’s function; (c)  $P_e$ ,  $P_l$ , and  $\eta$  as a function of  $V$ , when  $T_1 = 1000$  K and  $T_2 = 300$  K.

the planar system, a small unit cell (2 nm width) in x-direction is used, and periodic boundaries with Floquet periodicity are applied on the two ends, and we change the wavevector from 0 to  $200k_g$  in unit of  $k_g$ , while keeping the out-of-plane (y-direction) wavevector component as 0. This is sufficient to cover all  $k$  contributions due to the rotational symmetry of the system. Then the transmissivity is calculated for each  $k$  component from the resonant mode.

As shown in Fig. 2(a), the transmissivity recovers the SPP dispersion curve of a metal surface, with resonant frequency approaching  $2.12\omega_g$  at large  $k$ . The transmissivity peak due to the resonance diminishes for  $k$  larger than  $120k_g$ , as the effective wavelength increases, making photon tunneling through the gap more difficult. Summing over all  $k$  contributions, the transmissivity increases from lower frequency to a strong peak around  $2.12\omega_g$ , and drops rapidly at higher frequency (Fig. 2(b)), as no resonant mode is supported.

In Fig. 2(b), we also plotted the transmissivity from emitter obtained analytically. As we can see, the two curves almost coincide with each other except at smaller frequency, where the contribution to transmissivity is very low. Note that the resonance at small  $k$  is less confined, making it more difficult in accurately identifying the mode. Therefore it is not included in the transmissivity calculation. We have verified that this part contributes to a small amount of about 1% of the overall transmissivity and the exclusion does not affect of the overall accuracy of the calculation.

So we can see that although CMT is an approximation to the system by taking account only energy transferred through resonant modes, it is a suitable method for quantitative analysis of the performance of near-field TPV system.

At temperature  $T_1 = 1000$  K, the emitter power  $P_e$  is about  $11$  W/cm<sup>2</sup>. The power to the load as a function of voltage is also calculated, and the maximum converted electric power is about  $4$  W/cm<sup>2</sup>.

### 3.2 Nanostructured Emitter

For the system with periodically structured emitter, more than one resonant modes are supported and are labeled by band index  $n_x$ . The SPP mode is truncated by the periodicity and folded into multiple bands within the Brillouin zone. In addition, the metallic grating structures behave as leaky waveguides, and may support guided modes. The coupling between neighboring waveguides may form the so-called spoof SPP modes.<sup>37,38</sup>

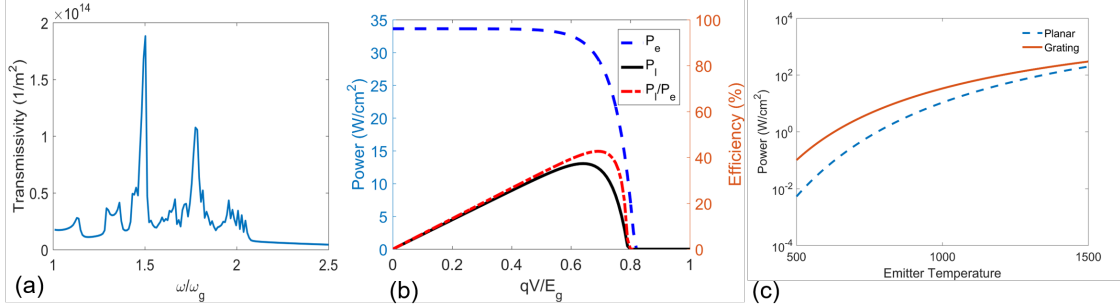


**Fig 3** Coupled-mode calculation results for the system with periodic structures: (a) transmissivity as a function of frequency; (b)  $P_e$ ,  $P_i$ , and  $\eta$  as a function of  $V$ , when  $T_1 = 1000$  K and  $T_2 = 300$  K; (c) Emitter power comparison of the two systems at different temperatures.

One unit cell in  $x$ -direction is modeled in the COMSOL solver, with Floquet wavevector  $k_x$  ranging from 0 to  $\pi/p$ , and 21 values are selected. For out-of-plane direction,  $k_y$  also varies from 0 to  $10\pi/p$ , with step size  $0.2\pi/p$ . Multiple resonant modes are obtained within the interested frequency range below the SPP resonance frequency of  $2.12\omega_p$ , which is reflected in the transmissivity curve as shown in Fig. 3(a). Note that for each  $k$  component, the first 5 resonances are extracted from the eigenfrequency solver, and used for the transmissivity calculation. As we see from the curve, the contribution to the transmissivity due to the first a few modes is the highest. This is because photons from lower order modes have longer wavelengths and can more easily tunnel through the gap between the emitter and PV cell. The same calculation process is done for power conversion and the result is plotted in Fig. 3(b), which shows a much larger emitted power ( $34 \text{ W/cm}^2$ ) and converted electric power ( $13 \text{ W/cm}^2$ ) compared with the planar system. The resonance modes supported by the structured emitter are lower in energy and thus better matched with the bandgap energy of the TPV cell, therefore the transmissivity and the power emission are both higher. The emitter power density and the enhancement effect strongly depend on the temperature of the emitter. As seen in Fig. 3(c), the ratio of output electric power from a grating based emitter can be 20 times as high as that from a planar emitter at temperature of 500 K. Although on the other hand, the power density drops rapidly with temperature.

The mode profile for each resonance can also be obtained from the eigenfrequency solver. The field distributions of the SPP mode of the grating system, and the first three modes of the nanostructured system are shown in Fig. 4. For the planar system, as seen in Fig. 4(a), the field is localized on the surface of the emitter, and decays to both sides. For the grating system, as shown in Fig. 4(b), (c), and (d), the field is also localized on the metal surface for each resonance. Each mode corresponds to a different order of SPP resonance, and each additional node appears at the grating surface for a higher order mode. It is noted that mode profiles are not required for the calculation process, and are only provided for understanding the resonances. Other than SPP modes, various resonant mechanisms may be supported with metallic nanostructures, such as localized surface plasmons, waveguide modes, spoof SPP modes, depending on the design parameters. With coupled-mode analysis, all resonant modes can be accounted for regardless of the physical mechanisms.

In order to further improve the performance, we want the structures to support resonant modes that are closer in energy to the bandgap of the PV cell. Therefore, the system performance depends

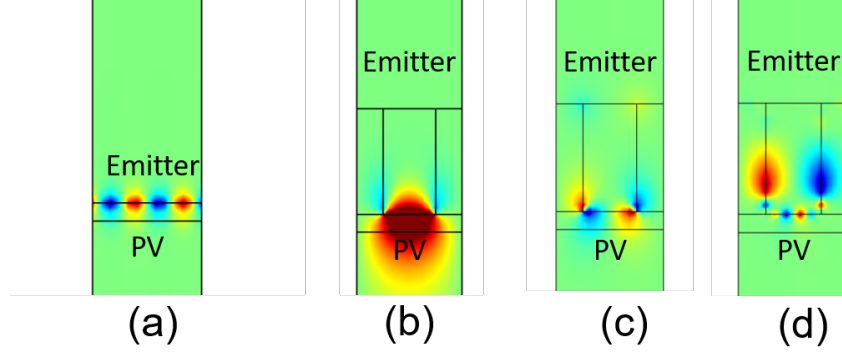


**Fig 4** Resonant mode profile that corresponds to (a) the SPP mode for the system with planar emitter, and [(b), (c), and (d)] the resonant modes corresponding to the three major transmissivity peaks at  $1.503\omega_g$ ,  $1.775\omega_g$ , and  $1.957\omega_g$ , respectively for the system with nanostructured emitter.

both on the emitter structure, and the PV cell material. For the resonant modes supported by the emitter, the dispersion of each mode depends on the material properties and geometrical parameters of the nanostructures, and the relation is different for different modes. While several different resonant modes are supported, it is not straightforward to obtain an optimal geometry for the TPV system. In general, the larger the periodicity of the grating, the lower the energy of the periodicity induced modes. However, when the periodicity is further increased, the modes may fall below the bandgap. The depth of the grating also changes the mode dispersion, if the depth is too shallow, some cavity resonances may not be supported. If the depth is too steep, most of the field may be focused in the cavity instead of near the surface of the emitter, causing weaker near field coupling.

The results shown in Fig. 3 is only an example to compare with the system with planar emitter, and the parameters are not optimized. Modification of the geometrical parameters can potentially improve the power generation. For example, when the periodicity  $p$  is changed to 90 nm, and  $w$  is changed to 45 nm, major transmissivity peaks are shifted to lower frequencies, and the resultant power density in the same temperature settings is increased to  $40 \text{ W/cm}^2$ . A numerical optimization process will be necessary to obtain the best parameters for the nanostructured TPV system.

#### 4 Conclusions

In summary, we developed a procedure to calculate the performance parameters of a near-field TPV system including transmissivity, radiation power, electric power, and efficiency based on coupled-mode analysis. CMT, although is considered an approximate approach, is suitable for the quantitative analysis of near-field thermophotovoltaic system with one or several surface resonant modes.

We applied the CMT-based calculation procedure for a near-field TPV system with planar emitter and a metallic grating based emitter. We showed that additional resonant modes introduced by metallic gratings are captured by CMT. These geometry-induced modes are lower in energy than the SPP mode supported by a planar surface, and therefore closer to the bandgap energy of a typical TPV cell. As we can see, nanostructures provide another degrees of freedom to improve the overall performance of the near-field based TPV system. The calculation process developed in this paper based on coupled mode analysis offers a new way to quantify the performance. The

method is especially useful for systems with complicated structures, where conventional methods may fail or takes too long to solve. We believe this work will help facilitate novel designs and offer a reliable approximation of the performance for near-field TPV systems.

### References

- 1 S. Basu, Z. M. Zhang, and C. J. Fu, “Review of near-field thermal radiation and its application to energy conversion,” *International Journal of Energy Research* **33**(13), 1203–1232 (2009).
- 2 I. S. Nefedov and C. R. Simovski, “Giant radiation heat transfer through micron gaps,” *Phys. Rev. B* **84**, 195459 (2011).
- 3 B. Guha, C. Otey, C. B. Poitras, *et al.*, “Near-field radiative cooling of nanostructures,” *Nano Letters* **12**(9), 4546–4550 (2012). PMID: 22891815.
- 4 P. Würfel and U. Würfel, *Physics of Solar Cells: From Basic Principles to Advanced Concepts*, Physics textbook, Wiley (2009).
- 5 *Thermophotovoltaics - Basic Principles and Critical Aspects of* | Thomas Bauer | Springer.
- 6 C. Ferrari, F. Melino, M. Pinelli, *et al.*, “Overview and status of thermophotovoltaic systems,” *Energy Procedia* **45**, 160 – 169 (2014). {ATI} 2013 - 68th Conference of the Italian Thermal Machines Engineering Association.
- 7 J. Park, S. Lee, H. Wu, *et al.*, “Thermophotovoltaic power conversion from a heat-recirculating micro-emitter,” *International Journal of Heat and Mass Transfer* **55**(1718), 4878 – 4885 (2012).
- 8 P. Davies and A. Luque, “Solar thermophotovoltaics: brief review and a new look,” *Solar Energy Materials and Solar Cells* **33**(1), 11 – 22 (1994).
- 9 C. Ungaro, S. K. Gray, and M. C. Gupta, “Solar thermophotovoltaic system using nanostructures,” *Opt. Express* **23**, A1149–A1156 (2015).
- 10 R. S. Tuley and R. J. Nicholas, “Band gap dependent thermophotovoltaic device performance using the ingaas and ingaasp material system,” *Journal of Applied Physics* **108**(8), 084516 (2010).
- 11 L. C. Chia and B. Feng, “The development of a micropower (micro-thermophotovoltaic) device,” *Journal of Power Sources* **165**(1), 455 – 480 (2007).
- 12 A. Lenert, D. M. Bierman, Y. Nam, *et al.*, “A nanophotonic solar thermophotovoltaic device,” **9**(2), 126–130.
- 13 Y. X. Yeng, W. R. Chan, V. Rinnerbauer, *et al.*, “Photonic crystal enhanced silicon cell based thermophotovoltaic systems,” *Opt. Express* **23**, A157–A168 (2015).
- 14 H. Sai and H. Yugami, “Thermophotovoltaic generation with selective radiators based on tungsten surface gratings,” *Applied Physics Letters* **85**(16), 3399–3401 (2004).
- 15 N. Nguyen-Huu, J. Pitoro, and M. Cada, “Wavelength-selective emitters with pyramid nanogratings enhanced by multiple resonance modes,” *Nanotechnology* **27**(15), 155402 (2016).
- 16 B. J. Lee, L. P. Wang, and Z. M. Zhang, “Coherent thermal emission by excitation of magnetic polaritons between periodic strips and a metallic film,” *Opt. Express* **16**, 11328–11336 (2008).
- 17 D. Polder and M. Van Hove, “Theory of radiative heat transfer between closely spaced bodies,” *Phys. Rev. B* **4**, 3303–3314 (1971).

- 18 A. Narayanaswamy and G. Chen, “Surface modes for near field thermophotovoltaics,” *Applied Physics Letters* **82**(20), 3544–3546 (2003).
- 19 K. Joulain, J.-P. Mulet, F. Marquier, *et al.*, “Surface electromagnetic waves thermally excited: Radiative heat transfer, coherence properties and casimir forces revisited in the near field,” *Surface Science Reports* **57**(34), 59 – 112 (2005).
- 20 E. Rousseau, A. Siria, G. Jourdan, *et al.*, “Radiative heat transfer at the nanoscale,” *Nat Photon* **3**, 514–517 (2009).
- 21 M. Laroche, R. Carminati, and J.-J. Greffet, “Near-field thermophotovoltaic energy conversion,” *Journal of Applied Physics* **100**(6), 063704 (2006).
- 22 X. Liu, L. Wang, and Z. M. Zhang, “Near-field thermal radiation: Recent progress and outlook,” *Nanoscale and Microscale Thermophysical Engineering* **19**(2), 98–126 (2015).
- 23 X. Liu and Z. Zhang, “Near-field thermal radiation between metasurfaces,” *ACS Photonics* **2**(9), 1320–1326 (2015).
- 24 Y. Yang and L. Wang, “Spectrally enhancing near-field radiative transfer between metallic gratings by exciting magnetic polaritons in nanometric vacuum gaps,” *Phys. Rev. Lett.* **117**, 044301 (2016).
- 25 O. Ilic, M. Jablan, J. D. Joannopoulos, *et al.*, “Overcoming the black body limit in plasmonic and graphene near-field thermophotovoltaic systems,” *Opt. Express* **20**, A366–A384 (2012).
- 26 R. Messina and P. Ben-Abdallah, “Graphene-based photovoltaic cells for near-field thermal energy conversion,” **3**, 1383.
- 27 K. Park, S. Basu, W. King, *et al.*, “Performance analysis of near-field thermophotovoltaic devices considering absorption distribution,” *Journal of Quantitative Spectroscopy and Radiative Transfer* **109**(2), 305 – 316 (2008). The Fifth International Symposium on Radiative Transfer.
- 28 S. Molesky and Z. Jacob, “Ideal near-field thermophotovoltaic cells,” *Phys. Rev. B* **91**, 205435 (2015).
- 29 M. Elzouka and S. Ndao, “Towards a near-field concentrated solar thermophotovoltaic microsystem: Part i modeling,” *Solar Energy*, – (2015).
- 30 S. Jin, M. Lim, S. S. Lee, *et al.*, “Hyperbolic metamaterial-based near-field thermophotovoltaic system for hundreds of nanometer vacuum gap,” *Opt. Express* **24**, A635–A649 (2016).
- 31 L. Zhu, S. Sandhu, C. Otey, *et al.*, “Temporal coupled mode theory for thermal emission from a single thermal emitter supporting either a single mode or an orthogonal set of modes,” *Applied Physics Letters* **102**(10) (2013).
- 32 A. Karalis and J. D. Joannopoulos, “Temporal coupled-mode theory model for resonant near-field thermophotovoltaics,” *Applied Physics Letters* **107**(14) (2015).
- 33 A. Karalis and J. Joannopoulos, ““squeezing” near-field thermal emission for ultra-efficient high-power thermophotovoltaic conversion,” *Scientific Reports* **6**, 28472 (- 2016/07/01/online).
- 34 C. Lin, B. Wang, K. H. Teo, *et al.*, “Application of impedance matching for optimal emitter/absorber design in a thermophotovoltaic system,” *Phys. Rev. Appl.* **7**, 034003 (2016).
- 35 J.-Y. Chang, Y. Yang, and L. Wang, “Tungsten nanowire based hyperbolic metamaterial emitters for near-field thermophotovoltaic applications,” *International Journal of Heat and Mass Transfer* **87**, 237 – 247 (2015).

- 36 X. L. Liu, T. J. Bright, and Z. M. Zhang, “Application conditions of effective medium theory in near-field radiative heat transfer between multilayered metamaterials,” **136**(9), 092703–092703–8.
- 37 H. Yao and S. Zhong, “High-mode spoof spp of periodic metal grooves for ultra-sensitive terahertz sensing,” *Opt. Express* **22**, 25149–25160 (2014).
- 38 X. Liu, L. Zhu, Q. Wu, *et al.*, “Highly-confined and low-loss spoof surface plasmon polaritons structure with periodic loading of trapezoidal grooves,” *AIP Advances* **5**(7), 077123 (2015).